Design and characterization of a portable fluorescence measuring system for the on-site monitoring of marine bio-constructors

Davide Cassanelli, *Member, IEEE*, Paolo Rossi, Elena Cenni, Stefano Cattini, *Member, IEEE*, Sara Righi, Roberto Simonini, Alessandro Capra, Luigi Rovati, *Member, IEEE*, Cristina Castagnetti

***Abstract*—Marine bio-constructors are put at risk by natural disturbances caused by climate change and anthropogenic stressors. Given their fundamental importance in marine ecosystems, it is essential to reverse this trend. In this regard, measurement techniques capable of early detecting alterations of marine colonies are essential. Traditional underwater surveys rely on in-situ observations performed by divers, and in the last decade, such analysis has been increasingly supported by photogrammetry. Despite the significant benefits brought by photogrammetry and the notable progress of computer vision, to date, no measurement techniques fully succeeded in the early detection of minor alterations in the state of health. In this regard, fluorescence imaging has the potential to support and improve both ecological and physiological assessments. Nevertheless, to date, its use in the underwater environment is mainly exploited for qualitative nature photography and much less for quantitative analysis aimed at extracting biological information. One factor limiting the widespread use of quantitative fluorescence imaging to monitor marine bioconstructors is that studies in the literature generally do not allow for metrological traceability. Fluorescence intensity is usually reported in arbitrary units derived from the intensity of the acquired images. This study aims to support the transition from qualitative imagery to quantitative fluorescence imaging. To this end, we proposed introducing a simple and effective traceability obtained by relating the fluorescence intensity recorded by the instrument to the sodium fluorescein concentration that would generate the same intensity, namely the equivalent fluorescein concentration. This makes measurement results independent of the specific measuring system, enabling research conducted by different groups to be synergised.**

***Index Terms*—Fluorescence, Biometry, Marine Bioconstructors, Change Detection, Underwater ROVs, Technologies for Environmental Measurement, Photonic Instrumentation and Measurement.**

I. Introduction

Bioconstructor species play a fundamental role as they create reefs that sustain an extremely high biodiversity, provide key ecosystem services to the global economy, and influence important ecological processes [1], [2]. Marine bioconstructors are thus protected globally by the Convention on Biological Diversity, and many species are reported in the International Union for the Conservation of Nature (IUCN) Red List of Threatened Species. Unfortunately, marine communities are still facing significant natural disturbances and anthropogenic stressors. In particular, habitat-forming corals are endangered by multiple large-scale and local pressures [3]. On one side, global warming and invasive predators threaten coral cover and reef complexity [4], [5]. On the other side, human-mediated impacts, such as marine pollution, overfishing, and physical damage caused by boat anchoring, constitute critical drivers of coral decline [6].

Detecting changes in bioconstructor species is critical to reversing the current downward trends of these ecosystems, fostering protection and restoration purposes.

Classic underwater surveys rely on in-situ observations and measures performed by specialized divers. To overcome all the limitations related to the on-site analysis carried out by operators, in the last decade, photogrammetric approaches have become increasingly widespread both for close-range and habitat-scale analyses [7]–[9]. In addition, Remotely Operated Vehicles (ROVs) are increasingly being used to carry out analyses in conditions that are dangerous for human operators. These instruments, operated by divers, make it possible to avoid risks due to rough seas or unfavorable diving conditions [10]–[12]. In recent years, the combined use of ROVs and photogrammetry has been considered to improve survey accuracy and keep operators safe [13], [14].

Despite the significant benefits brought by photogrammetry and the notable progress of computer vision, to date, no measurement method has fully succeeded in the early detection of minor alterations in the state of health. In this regard, the photogrammetric analysis could be assisted by the study of the autofluorescence produced by many species of marine bioconstructors. Indeed, underwater fluorescence imaging has the potential to improve both ecological and physiological assessments [15].

The use of (quantitative) fluorescence as an analysis and measurement method has been widely known for a long time and is widespread in many fields [16]–[18]. Biological laboratories are a typical example. In recent years, fluorescence analysis has found more and more applications, even outside the laboratories. For example, for on-site monitoring of the vegetative state of plants [19]–[21] and also for applications related to the marine environment [22]–[26].

The research was funded by University of Modena and Reggio Emilia under the 2022 FAR Mission Oriented Call, title of the project: "POSEIDON - Photogrammetry, Optical SEnsors, and unmanned underwater vehIcles for non-invasive large-scale monitoring of meDiterranean benthic cOmmuNities and habitats" (CUP E95F2100343000). The activities were also partially supported by the PRIN 2022 project titled: "EUPHROSYNE: Enhancing Underwater PHotogrammetRy, fluOreScence imagerY and deep learning solutions for monitoring the health status of mediterraNEan corals," funded by Next Generation EU - PNRR, Mission 4, Component 2 (CUP E53D23003980006). The authors gratefully acknowledge the Municipality of Nardò for its logistical support and hospitality throughout the sampling campaign.

The pioneering studies conducted by Roth et al. in 2013 [27] regarding the possibility of analysing the fluorescence of Green Fluorescent Proteins (GFPs) to estimate coral health decline and those conducted by Treibitz et al. in 2015 [15] regarding the potential of fluorescent imaging to support annotation, introduced fluorescence imaging also for the analysis of marine bioconstructors. Nevertheless, the application of fluorescence imaging in the field of marine bioconstructors remains predominantly associated with qualitative nature photography, with comparatively fewer applications observed in which fluorescence is used as a tool for colony analysis. Nonetheless, as introduced previously, fluorescence imaging can support the early detection of minor alterations in at least two aspects. On the one hand, simplifying the identification of bioconstructors in underwater images. Indeed, bioconstructions often have a similar color to the background, but, unlike the background, some of them are autofluorescent. Hence, it is easier to identify them in a fluorescence image rather than in a color image. On the other hand, quantitative GFP fluorescence imaging has been shown to be a powerful tool for estimating the health status of bioconstructors [27]–[29]. Furthermore, the possibility of measuring the fluorescence produced by chlorophyll contained in some symbiotic algae could further support the analysis of the health status of the colonies. Indeed, the concentration of chlorophyll is directly related to the photosynthetic efficiency of these symbionts and, consequently, to the metabolic resources available to the coral. Thus, the alterations in chlorophyll fluorescence may provide early indications of stress conditions [30]–[34] representing a key tool for monitoring coral health.

Notwithstanding this fact, the utilization of fluorescence imaging as a tool for marine bioconstructor health analysis remains extremely limited and, to the best of our knowledge, to date, no fluorescence intensity values or thresholds have been defined that can be used to classify the health status of corals. The absence of metrological traceability has been a significant obstacle to establishing such thresholds and, consequently, to the widespread implementation of fluorescence analysis for assessing bioconstructor health. As will be described in section II, the intensity of images acquired by the imaging system depends on the system used. Therefore, studies in the literature generally report fluorescence intensity in arbitrary units directly derived from the intensity of the acquired images. While this allows the analysis of variations within the specific study, it precludes comparison between measurement results obtained by different research groups using different measuring systems. This resulted in no homogeneous data available in the literature on which to base objective thresholds for assessing the health of bioconstructors.

To address the aforementioned limitations, this study proposes a simple and effective procedure to establish metrological traceability. Such a method is based on relating the fluorescence intensity of the images acquired by the measuring system to a measurement standard, namely the concentration of sodium fluorescein that would have generated the same fluorescence intensity. The objective is allow the consistency of results across different measuring systems and facilitate collaboration between multiple research groups. To the best of our knowledge, this is the first study addressing metrological traceability in the analysis of fluorescence generated by bioconstructors.

In addition, in the present study, the measuring system has been completely re-engineered with respect to the previous versions [28], [29], to enable the analysis of the fluorescence intensity produced by symbiotic algae, thereby allowing the acquisition of substantially more comprehensive information.

In the following, section II describes the developed measuring system prototype, the proposed image analysis and the performed metrological characterization. Section III reports some example results obtained from *Cladocora caespitosa* colonies. Finally, section IV proposes some final discussion and conclusions.

II. Materials and methods

As long as the fluorophore concentration in the sample is low, a fairly common condition when the fluorophore is endogenous, the radiant power (or radiant flux), Φ_{fluo}, generated by fluorescence is a monotonic increasing function of the fluorophore concentration [35]. The radiant power, Φ_{fluo}, also linearly depends on the quantum yield of the fluorophore and, for low fluorophore concentrations, is a monotonic increasing function also of the optical power absorbed by the fluorophore [35]–[37]. Therefore, as long as the fluorophores in the sample are not too concentrated and the irradiance of the excitation source, E_{ex}, is low enough, Φ_{fluo} grows as the concentration of the fluorophores and E_{ex} increases. Hence, Φ_{fluo} can be correlated with the fluorophore concentration thus with health status.

In the following, Subsection II-A describes the developed measuring system prototype, also briefly reporting some design rules to take into account. Then, Subsection II-B reports the proposed measurement method. Subsection II-C describes the metrological characterisation of the proposed measuring system, focusing particularly on the procedure for achieving metrological traceability — namely, the use of measurement standards composed of fluorophore solutions at known concentrations. Finally, subsection II-D describes the procedure for analyzing bioconstructors.

A. The developed measuring system prototype

The proposed measuring system must comply with certain specific constraints and design rules. Its design started from the study of fluorescence related to aquatic organisms of interest (bio-constructors), and then subsequently, the system was integrated with an ROV (BlueROV2 by Blue Robotics Inc, US).

Since GFP-like proteins concentration is considered to be correlated with corals state of health, the proposed measuring system is aimed at measuring the fluorescence intensity generated by GFP-like proteins. In addition to GFP-like proteins, it is also important to consider chlorophyll, as it is contained within the endosymbiotic algae (zooxanthellae) associated with corals.

GFP has an excitation peak at approximately 488 nm. Thus, the proposed system excites fluorophores using LED sources

that emit in this spectral region around 470 nm (blue).
Chlorophyll has an excitation peak at approximately 420 nm. Thus, to excite also the chlorophyll present in seaweed, the proposed system is equipped with LED sources designed to emit within the spectral region around 405 nm (violet).
Considering that the emission maxima of fluorescence produced by GFP and Chlorophyll are approximately 510 nm and 690 nm, respectively, fluorescence imaging was design to be conducted utilizing a conventional (silicon) camera.
Neglecting noise, the intensity, g, of the (x, y) pixel of the photosensors array is given by [38]:

$$g(x,y) = \int_{t_{exp}} \int_{A_{pix}} \int_{\Delta\lambda} R_\lambda(\lambda) \cdot E'_\lambda(x,y,\lambda) \, \mathrm{d}\lambda \, \mathrm{d}A_{pix} \, \mathrm{d}t \ , \tag{1}$$

where, t_{exp} is the exposure time of the camera pixel, A_{pix} is the (effective) pixel area, $E'_\lambda(x, y, \lambda)$ is the (average) spectral irradiance impinging on the (x, y) pixel, $\Delta\lambda$ is the spectral irradiance band and, $R_\lambda(\lambda)$ is the photosensor spectral responsivity at wavelength λ.
Since $E'_\lambda(\lambda)$ depends on the spectral radiant power, $\Phi'_\lambda(\lambda)$, collected by the imaging system, the grey level can be correlated with the radiant power, thus Φ_{fluo}.
One of the main critical issues related to quantitative fluorescence imaging is given by the fact that the radiant power generated by fluorescence, Φ_{fluo}, is generally very weak and, therefore, in the absence of particular attention, the spectral irradiance impinging on the pixel, $E'_\lambda(\lambda)$, depends only marginally on the quantity intended to be measured, i.e., Φ_{fluo} thus, the fluorophores concentration.
The overall radiant power impinging on the aperture of the imaging system is fundamentally given by three contributions that add together:

- the radiant power generated by the fluorescence, Φ_{fluo} (the quantity intended to be measured)
- the radiant power generated by the reflection and backscattering of the radiation used to excite the fluorophores, $\Phi_{ex-back}$ (the blue LEDs) and,
- the radiant power generated by the reflection and backscattering of the ambient lighting, $\Phi_{am-back}$.

As is well known in fluorescence microscopy, the radiant power $\Phi_{ex-back}$ due to the reflection and backscattering of the radiation used to excite the fluorophores is generally significantly greater (typical, two or three orders of magnitude) than the radiant power generated by the fluorescence — Φ_{fluo}. Therefore, it is common to employ interference filters to minimize the amount of radiant power due to the reflection and backscattering of the radiation used to excite the fluorophores that can reach the camera pixels. In particular, excitation filters were used to prevent the radiation used to excite the fluorophore from containing spectral components in the band of the emitted fluorescence signal. Similarly, the radiation that reaches the detector was filtered using an emission filter to allow only radiation in the spectral region of the fluorophore emission to pass. The excitation and emission interference filters commonly used in fluorescence microscopy provide excellent transmission of the desired wavelengths (typically, greater than 90 %), with a sharp spectral cutoff and low transmission at other wavelengths (typically, less than 0.001 %).
This is the first significant difference between fluorescence imaging aimed at estimating the state of health using the quantitative analysis of fluorescence intensity and fluorescence imaging for nature photography purposes. Colored filters are often used for nature photography, allowing much of the radiation used to excite the fluorophores to reach the camera's pixels. As an example, Figure 1 shows the absorption and emission spectra of GFP, while Figures 2 and 3 show the transmissions of the (thin-film) interference filters used in the proposed system and of color filters commonly used for nature photography of coral fluorescence, respectively. As evident from the comparison between Figures 2 and 3, while interference filters significantly reduce the amount of radiant power due to the reflection and backscattering of the radiation used to excite the fluorophores that can reach the camera pixels (with attenuation typically of at least 5 orders of magnitude), the colored filters used for nature photography allow a large part of the excitation radiation to reach the sensor. Images obtained with these colored filters are thus brighter and more scenic, but with reduced information content.
As will be described in more detail in Subsection II-B, the sharp band obtained using an interferential emission filter also contributes to reducing the radiant power, $\Phi_{am-back}$, generated by the reflection and backscattering of the ambient lighting that reaches the pixels. Moreover, the impact of environmental light was minimized by capturing images in the absence of LED illumination and subsequently subtracting these images to eliminate the effects of ambient light.

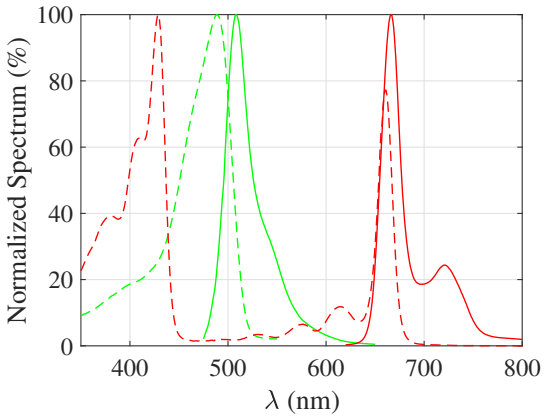

Fig. 1. Absorption (– –) and emission (—) spectra of GFP and absorption (– –) and emission (—) spectra of Chlorophyll (data from https://www.fpbase.org/protein/egfp/).

As previously introduced, the proposed system must be integrated in an underwater ROV, the BluROV2. Thus, it must be compact and with a particular design to be fit into the cylindrical enclosure provided by the ROV manufacturer. Figure 4 shows a drawing of the prototype system. The system uses a ring-illuminator layout. The camera was thus positioned on the system axis, with the light sources arranged around. All the components were placed inside a 3" acrylic cylindrical enclosure supported by 3D printed structures. The LEDs were arranged in a circular pattern, alternating blue and violet,

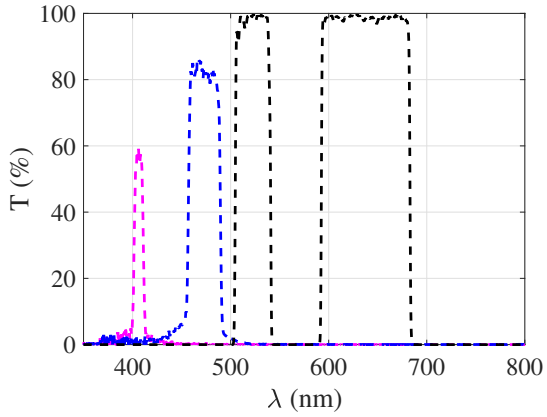

Fig. 2. Transmittance of the GFP excitation (..), Chlorophyll excitation (..) and dual band emission (−−) interference filters used to create the prototype.

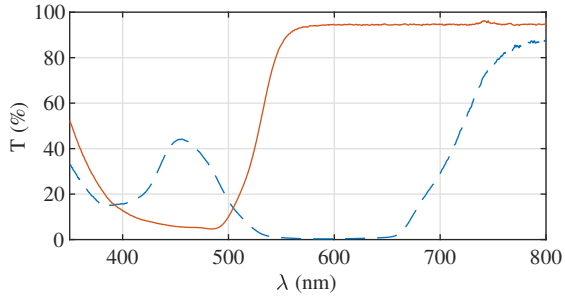

Fig. 3. Transmittance of excitation (−−) and emission (—) colored filters commonly used for nature photography of coral fluorescence.

consisting of 10 blue and 10 violet LEDs in total. The blue LEDs have an emission peak at 470 ± 10 nm, while the violet LEDs have an emission peak at 405 ± 5 nm. The excitation filters were placed upon the LED with another support. The support structure for the LED and filter was designed with a central aperture to accommodate the camera and the emission filter. A Python program operating on a Raspberry Pi 5, housed within the enclosure, manages the LED switching and captures images from the camera. In particular, the switching on of the LEDs was driven by a custom electronic board, ensuring consistent optical power output from the LEDs during successive switching phases.

Given that the camera optics employed for the acquisition of fluorescence images possess a fixed focal length, to facilitate the achievement of focus during ROV manoeuvres, the device incorporates a targeting system comprising two red lasers positioned above and below the camera. These lasers were angled so that their spots converge in the focal plane of the camera, located 110 cm away.

Communication with the remote PC was carried out via a Fathom-X Tether Interface Board. The list of all the components used to create the prototype is reported in Table I. The whole system can be powered directly by the ROV battery.

B. The proposed measurement method

As described previously, the used interference filters allow to minimize the contribution of the radiant power generated by

TABLE I
BILL OF MATERIALS.

Component	Model, Manufacturer
Blue LEDs	SMB1N-D470-02, Roithner Laser GmbH
Violet LEDs	SMB1N-D405-02, Roithner Laser GmbH
Camera	BFS-U3-50S5C-C, Flir
Objective Lens	M23F16V, Tamron
GFP Excitation Filter(s)	Custom
Chlorophyll Excitation Filter(s)	Custom
Emission Filter	59009m, Chroma Technology Corp
ROV	BlueROV2 Heavy Configuration Blue Robotics
Battery	Lithium Polymer Battery (14.8 V, 10 Ah)
Enclosure	3" Acrylic Watertight Enclosure, Blue Robotics
Dome	3" Optically Clear Acrylic Dome, Blue Robotics
On-board PC	Raspberry Pi 4
Ethernet connection	Fathom-X, Blue Robotics
LEDs driver	Custom electronic board
Pointing Laser(s)	LDM650/5LJM, Roithner Laser GmbH

the reflection and backscattering of the radiation used to excite the fluorophores, $\Phi_{ex-back}$ (the LEDs), as well as limiting to the spectral band of the emission filter the contribution due to the radiant power generated by the reflection and backscattering of the ambient lighting, $\Phi_{am-back}$. Although filtered by the emission filter, the contribution due to ambient lighting can still be significant. To enable the use of the system even in the presence of significant ambient lighting, the implemented measurement method involves the acquisition of two sets of images in rapid succession (< 0.1 ms between a shoot and the successive). In the first phase, called dark, N_{img} images were acquired while keeping the LED source off. Then, in the second phase, called excitation, the LED sources were turned on, first the blue and then the violet, and N_{img} images were acquired in rapid succession for each LED color (BLUE and VIOLET).

The dark acquisition phase is used to compensate for the minimal excitation of fluorophores caused by ambient light and the effects of the light itself. On the other hand, the intensity of the images recorded during the excitation phase depends on both the fluorescence generated by the sample and the reflection and backscattering of ambient lighting. Carrying out an average pixel by pixel, from each of the two sets of images acquired in the dark and excitation phases at time t, we obtained the average images $\bar{g}_{ex-GFP}(x, y, t)$, $\bar{g}_{ex-CHL}(x, y, t)$ and $\bar{g}_{dark}(x, y, t)$. Since GFPs have excitation and emission peaks at around 488 nm and 508 nm respectively, $\bar{g}_{ex-GFP}(x, y, t)$ is the average value of the intensity of the green pixel (x, y) calculated on the N_{img} images acquired when the blue LEDs were on. Similarly, since chlorophyll has an excitation peak at approximately 420 nm and an emission peak at around 670 nm, $\bar{g}_{ex-CHL}(x, y, t)$ is the average value of the intensity of the red pixel (x, y) calculated on the N_{img} images acquired when the violet LEDs were on. $\bar{g}_{dark}(x, y, t)$ is the average value calculated when all LEDs were off considering only the green pixels for GFPs and only the red pixels for chlorophyll. Then, in the hypothesis that the contribution due to environmental lighting remains substantially constant between the two

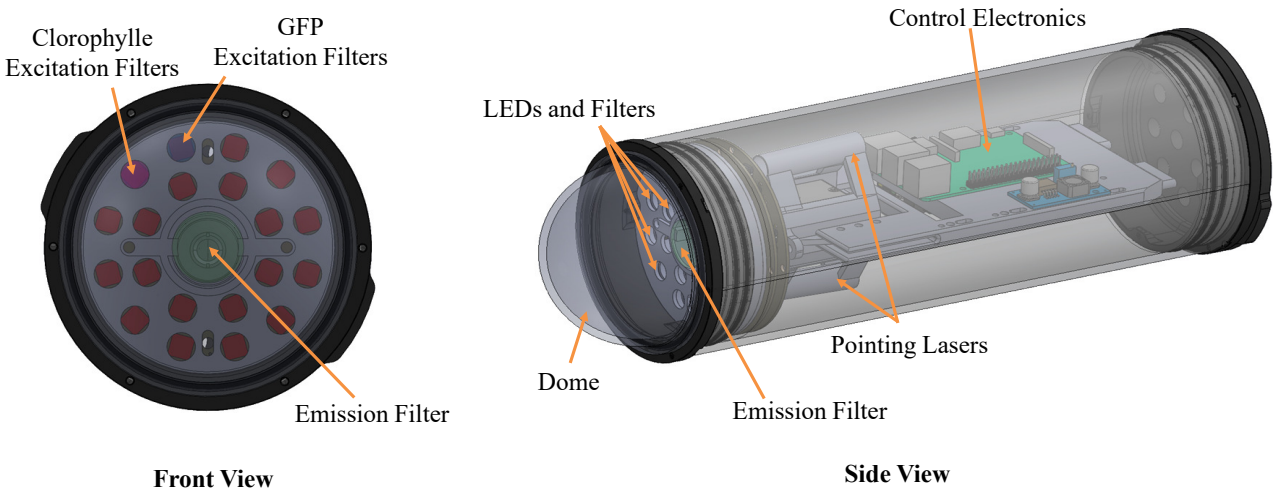

Fig. 4. Drawing of the prototype system. The targets are excited using the blue and violet LEDs. The excitation filters were used to prevent the radiation generated by the LEDs from containing spectral components in the band of the fluorescence emitted by the fluorophores. Indeed, the radiation used to excite the fluorophores is also reflected and backscattered by the target. It was therefore essential to minimize the spectral component of this radiation that would fall within the passband of the emission filter positioned in front of the camera. Then, the emission filter ensures that the radiation that reaches the detector nominally contains only the spectral band relating to the emission of the fluorophores. In addition, two pointing lasers were added to easily found the focal point during the underwater operation.

subsequent dark and excitation phases, intensities nominally due to fluorescence only, $\bar{g}_{fluo-GFP}(x,y,t)$ and $\bar{g}_{fluo-GFP}$, were estimated as:

$$\begin{aligned}\bar{g}_{fluo-GFP}(x,y,t) &= \bar{g}_{ex-GFP}(x,y,t) - \bar{g}_{dark}(x,y,t)\\ \bar{g}_{fluo-CHP}(x,y,t) &= \bar{g}_{ex-CHP}(x,y,t) - \bar{g}_{dark}(x,y,t)\ .\end{aligned} \tag{2}$$

Compensation for the contribution due to ambient lighting is another relevant difference compared to what is typically done in fluorescence nature photography.

The estimate made in (2) is the difference between the values recorded in the two phases. Thus, to be effectively descriptive of the fluorescence signal, it is necessary that not only the ambient lighting remain constant between the two phases but also that the camera settings remain unchanged, as well as that all the non-linear functions implemented by the camera are disabled (e.g., Gamma correction). The acquisition of N_{img} images made it possible to subsequently evaluate the reasonableness of the hypothesis regarding the substantial constancy of environmental lighting.

C. Characterization of the Proposed Measuring System

The characterization of the measuring system investigated: metrological traceability, warm-up and stability, repeatability and detection limit (minimum detectable equivalent fluorescein concentration).

1) Metrological traceability: As previously introduced, despite the design considerations described in subsection II-A, the intensity, g recorded by the imaging sensor depends inexorably on the characteristics of the system used. Therefore, in the absence of metrological traceability, the intensity recorded with one system cannot generally be compared with that obtained using another system. However, being able to compare measurement results is essential to fully exploit the potential of fluorescence imaging for marine bioconstructors monitoring. To this end, in this study we propose referencing the intensity recorded by the imaging sensor to a standard, that is, the fluorophore concentration that would have produced the same intensity.

As a reference fluorophore, we propose using sodium fluorescein. Sodium fluorescein is readily available, safe (it is not classified as a corrosive/irritant), readily soluble in water, and stable. In addition to these characteristic features, sodium fluorescein exhibits other properties that are essential for the reference fluorophore. Indeed, the reference fluorophore must have absorption and emission bands such that both the GFP and the chlorophyll measuring subsystem can excite the reference fluorophore and detect the resulting fluorescence. In other words, the absorption and emission bands of the reference fluorophore must at least partially overlap with those of the target fluorophores (GFP and chlorophyll, respectively). This is true for fluorescein.

In case a single reference fluorophore is not able to provide such overlaps, the characterization of the two subsystems would have simply required the use of two different standards, that is, two different fluorophores, one for the GFPs subsystem and the other for the chlorophyll subsystem.

In order to achieve traceability, nine reference samples were prepared in buffer solution at different concentrations of fluorescein, ranging from 0.1 μmol/L to 2.5 μmol/L. The selected range of concentrations was determined based on the fluorescence intensities expected from marine bioconstructors. Moreover, concentrations within this range are sufficiently low to mitigate occurrences such as self-absorption, thereby ensuring a linear relation between the fluorophore concentration and the resultant fluorescence intensity. The samples were prepared inside a fluorescence cuvette and placed at the focus distance $d = 1.1$ m of the camera from the instrument.

For each sample, the measurement procedure proposed in Subsection II-B was followed, thus acquiring $N_{img} = 5$

images with the LED source switched off, then $N_{img} = 5$ images with the blue LEDs switched on, and $N_{img} = 5$ images with the violet LEDs switched on.

The images were processed to obtain $\bar{g}_{ex-F}(x, y, C)$, $\bar{g}_{dark}(x, y, C)$ and $\bar{g}_{fluo-F}(x, y, C)$, where C is the fluorescein concentration, and F stays for each fluorophore GFP and CHP, as in (2). Then, the fluorescence intensity of the sample $\bar{g}_{fluo-m-F}(C)$ was computed by computing the mean vale of the average image $\bar{g}_{fluo-F}(x, y, C)$, by considering only the image area corresponding to the cuvette as in (3).

$$\bar{g}_{fluo-m-F}(C) = \frac{1}{M \cdot Q} \sum_{x=1}^{M} \sum_{y=1}^{Q} \bar{g}_{ex-F}(x, y, C) \cdot \frac{100}{2^{16} - 1} \ . \tag{3}$$

The fluorescence intensity values are reported as percentages of the maximum range of pixel depth after saving the images, specifically 16-bit. To provide an idea about the accuracy of the $\bar{g}_{fluo-m-F}(C)$ estimation, experimental standard deviation of the mean σ_{g-F} was computed among all the pixel intensity values. The values of $\bar{g}_{fluo-m-F}(C)$ were used to fit two linear models, $f_{GFP}(C)$ and $f_{CHP}(C)$, which relate the fluorescein concentration to the light intensity recorded by the two subsystems (the one responsible for measuring GFPs and the one for chlorophyll). Figure 5 shows the results of this test for both the fluorophores. The models exhibit sensitivities of $m_{GFP} = 9.7$ %/(μmol/L) for GFP and $m_{CHP} = 0.9$ %/(μmol/L) for Chlorophyll, respectively. The error-bars represent $2\sigma_{g-F}$. When analyzing the chlorophyll model, the some points present error bars extending into negative values. This effect arises from the zero adjustment performed with the dark reference image $\bar{g}_{dark}(x, y, C)$.

2) Warm-up and stability: The proposed measurement procedure, outlined in subsection II-B, involves the acquisition of two sets of images in rapid succession (< 0.1 ms between one shot and the next). In the first phase, N_{img} dark images are acquired. In the second phase, N_{img} images are acquired with both the blue LEDs alone and the violet LEDs alone turned on. Following this, the system will enter a $T_{idle} = 120$ s period before repeating the procedure in a loop. To speed up the warm-up, before using the measuring instrument, both the blue and violet LEDs are turned on continuously for a period of time $T_{blue-warm}$ and $T_{violet-warm}$, respectively. These times have been defined hemipyrically as $T_{blue-warm} = 180$ s and $T_{violet-warm} = 120$ s. Therefore, 60 s after the blue LEDs were activated, the violet LEDs were also activated so that, at the end of $T_{blue-warm} = 180$ s, the violet LEDs had also completed $T_{violet-warm} = 120$ s.

Figure 6 shows the results obtained by the two subsystems (GFPs and chlorophyll) analyzing a sample of sodium fluorescein and starting from the system turned off for at least 4 hours. The analysis observed a time span of about 150 min; a value higher than the battery life of the ROV used (the battery life of the BlueROV2 Heavy Configuration in 'normal use' is declared equal to approximately 2 h. Presumably due to the added components, the system in use rarely reached 90 min). As shown in Figure 6, considering a ± 1 % threshold, both subsystems have a warm-up time that does not exceed $T_{warm-up} = 26$ min.

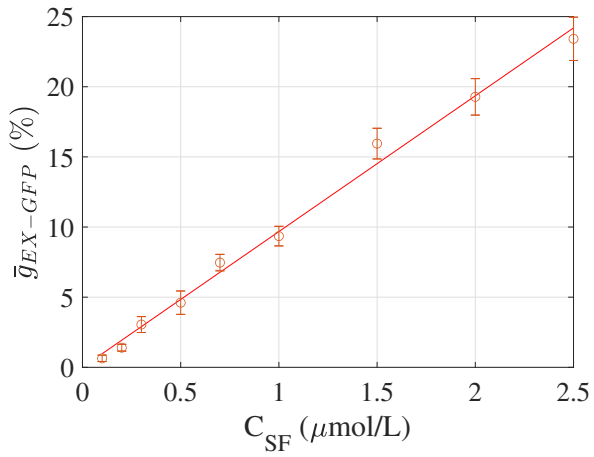

(a)

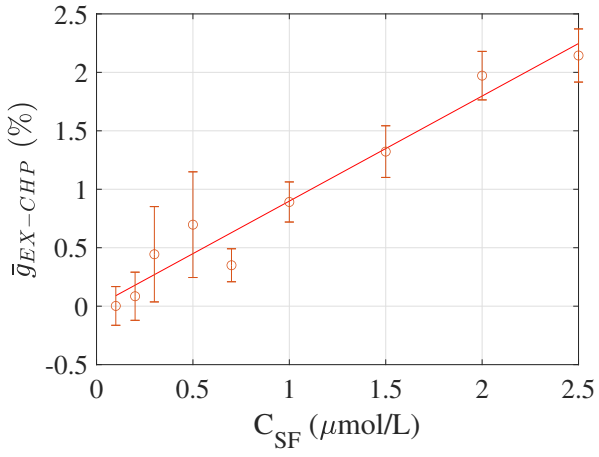

(b)

Fig. 5. Results of system characterization for both the fluorophore. On the x-axis, there is the fluorescein sample concentrations, while on y-axis the obtained mean intensity $\bar{g}_{fluo-m-F}(C)$. The orange circles ○ represent the experimental points obtained during the test, while the error-bars represent the twice experimental standard deviation of the mean $2\sigma_{g-F}$. The solid red lines — represents the linear models obtained with the experimental points. The models slopes are $m_{GFP} = 9.9$ %/μmol/L for GFP and $m_{CHP} = 0.9$ %/μmol/L for Chlorophyll, respectively. Figure (a) shows the results for the GFP ($\bar{g}_{fluo-m-GFP}(C)$), while Figure (b) shows the results for the Chlorophyll ($\bar{g}_{fluo-m-CHP}(C)$). The error-bars present negative value due to the subtraction of the dark image $\bar{g}_{dark}(x, y, C)$.

The tests shown in Figure 6 concerned short-term stability, that is, stability within a single measurement session. With regard to long-term stability, the stability and portability of fluorescein samples is such that they can also be used for calibration verification. In this regard, it is important to remember that the pH of buffer solutions is temperature-dependent and that the pK_a of fluorescein depends on pH. Therefore, it is advisable to take into account the potential effect of temperature and keep the samples tightly sealed to prevent evaporation and pH alteration by the environment.

3) Repeatability: Repeatability was investigated using the following procedure:

1) The instrument was left off for $T_{off} = 4$ h.
2) The instrument was turned on and the warm-up rou-

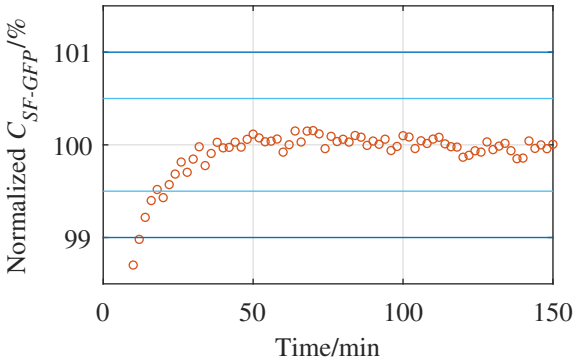

(a) Equivalent fluorescein concentration estimated by the GFPs subsystem (normalized to the steady-state value).

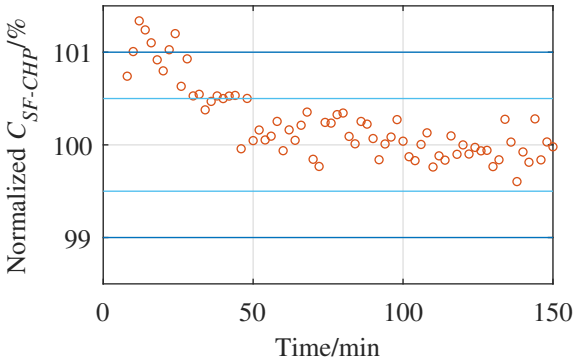

(b) Equivalent fluorescein concentration estimated by the chlorophyll subsystem (normalized to the steady-state value).

Fig. 6. Warm-up and stability of the two subsystems (GFPs and chlorophyll) obtained by analyzing a sodium fluorescein sample. In the figure, time instant 0 is defined by the end of the continuous LED lighting phase (i.e. by the simultaneous conclusion of $T_{blue-warm}$ and $T_{violet-warm}$).

tine was implemented (turning on the blue LEDs for $T_{blue-warm} = 180$ s and, after 60 s from the lighting of the blue LEDs, also turning on the violet LEDs for a total time of $T_{violet-warm} = 120$ s).

3) Start the acquisition routine. Acquisition of two sets of images (N_{img} dark images and N_{img} images with both the blue LEDs alone and the violet LEDs alone turned on) followed by a $T_{idle} = 120$ s period.
4) Repeat step '3)' 15 times and record only the last 3 acquisitions (the first 12 acquisitions were considered for warm-up and therefore discarded).
5) repeat the procedure starting from point '1)'.

The results obtained are shown in Figure 7.

4) Detection limit: Minimum Detectable Equivalent Fluorescein Concentration. The performance of the proposed measuring system depends on intrinsic characteristics, such as the noise of the sensor used, and heavily depends on environmental conditions, particularly in terms of environmental illumination (intensity and stability). Given the interest in field applications, environmental parameters are likely to have a not negligible impact on attainable performance. Therefore, given that each session will generally have (slightly) different environmental conditions, it is to be expected that each measurement session will have a different detection limit. Such a value will also generally be different for the two subsystems (GFPs and chlorophyll). This hypothesis is confirmed by the experimental results which will be reported in Table II.

In order to estimate the detection limit for a specific measurement session, we thus propose calculating the Minimum Detectable Equivalent Fluorescein Concentration (MEFC) $MEFC_{SF-F}$. It represents the lowest theoretically measurable value of $C_{SF-F}(x,y,t)$ that can be detected. To calculate $MEFC_{SF}$, a pixel-by-pixel variance $\sigma^2_{dark}(x,y,t)$ is determined from each dark image within a collection of images, resulting in a variance matrix as in:

$$\sigma^2_{dark}(x,y,t) = \\ = \frac{1}{N_{img}-1}\sum_{k=1}^{N_{img}}\left(G^{(k)}_{dark}(x,y,t) - \bar{G}_{dark}(x,y,t)\right)^2 . \quad (4)$$

where $G^{(k)}_{dark}(x,y,t)$ represent the k-th dark images of a single set of acquisition at time t. Subsequently, the square root of the mean value of $\sigma^2_{dark}(x,y,t)$ is calculated to derive the standard deviation of the mean dark images $\sigma_{dark}(t)$. This calculated parameter quantifies the minimum detectable light intensity with respect to pixel intensity. Nonetheless, it is advantageous to convert this parameter into equivalent concentration terms by applying the model as referenced in (5) to obtain $MEFC_{SF-F}$. $MEFC_{SF-F}$ must be computed for each set of acquisitions, since the environmental conditions can mutate.

D. Bio-constructor Analysis

The study of marine bio-constructors was carried out by the analysis of the images acquired through the measurement method described in Subsection II-B. The analysis of the acquired images was performed by extracting the following parameters from the intensities, $\bar{g}_{fluo-F}(x,y,t)$ obtained, where the suffix F stays for GFP or Chlorophyll:

- Calculation of the equivalent sodium fluorescein concentration $C_{SF-F}(x,y,t)$, as well as its average across the entire image $\bar{C}_{SF-F}(t)$. This parameter indicates the concentration of sodium fluorescein required in the bio-constructor to achieve a particular light intensity captured by the camera. $C_{SF-F}(x,y,t)$ is computed by reverting the models derived in the characterization phase described in Subsection II-C. Specifically, the equivalent concentration is computed as:

$$C_{SF-GFP}(x,y,t) = f'_{GFP}(\bar{g}_{fluo-GFP}(x,y,t)) \\ C_{SF-CHP}(x,y,t) = f'_{GFP}(\bar{g}_{fluo-CHP}(x,y,t)) . \quad (5)$$

  It ensures a standardized measurement, unaffected by environmental conditions or camera configurations.

- Total number of pixels, $N_{pixel-F}(t)$, in the $C_{SF-F}(x,y,t)$ image above a threshold value, C_{th-F}. Such a threshold had been empirically determined by analysing the average $C_{SF-F}(x,y,t)$ in the image in which a corallite was not contained (portion of image with no fluorescence). The $N_{pixel-F}(t)$ estimator can potentially detect a decrease in fluorescence by

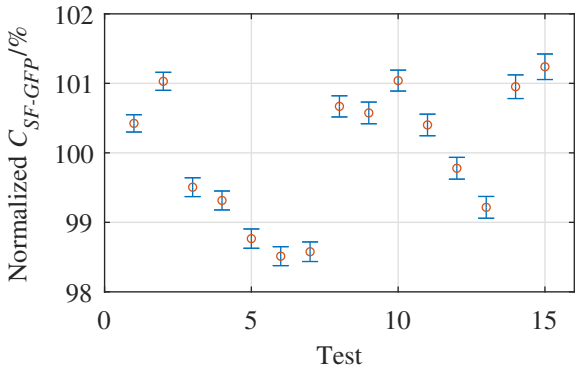

(a) Equivalent fluorescein concentration estimated by the GFPs subsystem (normalized with respect to the mean value obtained in the tests). For each test, the bars represent the experimental standard deviation of the mean calculated on the N_{img} images. The experimental standard deviation obtained from the analysis of mean values obtained from the 15 tests is 0.95 %.

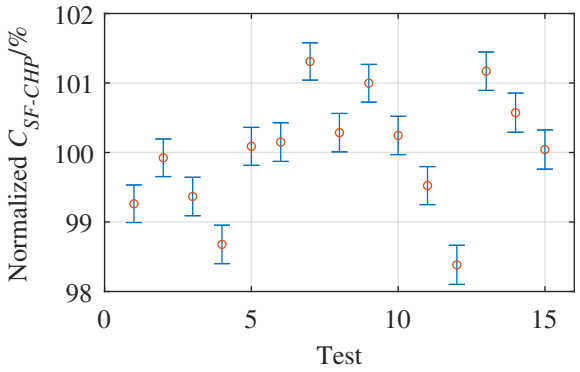

(b) Equivalent fluorescein concentration estimated by the chlorophyll subsystem (normalized with respect to the mean value obtained in the tests). For each test, the bars represent the experimental standard deviation of the mean calculated on the N_{img} images. The experimental standard deviation obtained from the analysis of mean values obtained from the 15 tests is 0.85 %.

Fig. 7. Repeatability of the two subsystems (GFPs and chlorophyll) obtained by analyzing a sodium fluorescein sample.

quantifying the total number of pixels exceeding the threshold. These pixels are presumed to be associated with the fluorescence signal. Such a decrease may indicate a reduction in the surface area of polyps, caused by factors like partial closure or health deterioration, or a rise in the number of unhealthy corals.

- The Mean Equivalent Fluorescein Concentration, $\bar{C}_{SF-F}(t)$, refers to the concentration of pixels in the image $C_{SF-F}(x, y, t)$ that exceed the threshold C_{th-F}. By assessing the intensity of these fluorescent pixels, which are those surpassing the threshold, the $\bar{C}_{SF-F}(t)$ estimator has the potential to offer additional insights into the health status of the bio- constructors.

III. Example Results

In order to verify the ability of the proposed measuring system and methods, live colonies of *Cladocora caespitosa* were analysed. *Cladocora caespitosa* is the most important reef-building species in the Mediterranean and is also included in the Red List of the International Union for the Conservation of Nature (IUCN).

Coral fragments were collected among those naturally detached from the substrate after sea storms. The samples thus collected were taken to the laboratory in aquarium where temperature ($[18, 20]$ °C), salinity ($[36, 38]$ %), and photoperiod (12 h light and 12 h dark by LED lighting) were kept monitored. We perform a test on two different coral fragments, namely, C1 and C2. The test regards the acquisition and analysis of fluorescence information of the corals placed in seawater. The measuring instrument was aligned with the coral at a distance of $d = 1.1$ m. The test procedure regards the acquisition of $N_{img} = 5$ DARK, BLUE and VIOLET images. After the acquisition phase, the images were analyzed to retrieve the minimum detectable equivalent fluorescein concentration $MEFC_{SF-F}$ to set the concentration threshold C_{th-F}. Then the proposed metrics $N_{pixel-F}$, $\bar{C}_{SF-F}(t)$ and $C_{SF-F}(x, y, t)$ have been evaluated. As an example, Figure 8 shows three images acquired during the dark and subsequent excitation phases (BLUE and VIOLET), respectively. The images exposition was enhanced to improve their visualization for the reader.

Table II show the average values of N_{pixel} and $\bar{C}_{SF-F}(t)$ obtained for each excitation light and for each coral together with $MEFC_{SF-F}$ and the concentration threshold for both the corals and both fluorophores, C_{th-F}.

The inverted linear model shown in Figure 5 was applied to the images shown in Figure 8 to estimate the equivalent fluorescein concentrations. Figure 9 shows the results of such analysis.

The measurement results obtained using the proposed measuring system were thus compared with visual analysis performed by biologists, currently the only available method for analysing marine bioconstructor.

As previously mentioned, fluorescence imaging can be a valuable aid in identifying bioconstructors in underwater images and in analysing alterations in their health status. The primary purpose of the comparison with the visual analysis performed by biologists was to verify that the structures highlighted by the fluorescence analysis were indeed those of interest. As clearly shown in Figures 8 and 9, this feature was fully confirmed.

With regard to the estimation of health status, while biologists confirmed that the analysed samples were healthy and the high fluorescein equivalent values recorded by the proposed measuring instrument suggested such a state of health, no fluorescence intensity values or thresholds have been defined in the literature that can be used to classify the health status of corals. Consequently, at present, fluorescence intensity analysis can provides valuable support for analysing changes in health status, but it is not yet able to provide an estimate of absolute health status. The primary objective of this study is to propose a practical method to introduce traceability, contributing to address this gap.

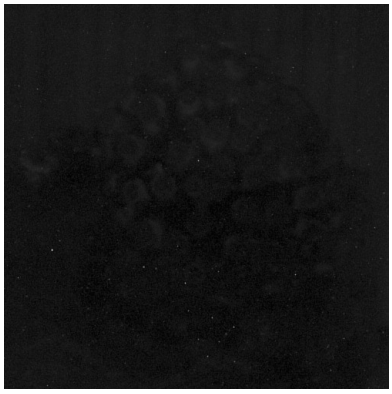

(a) Dark.

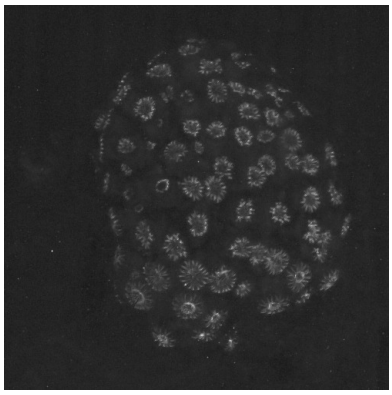

(b) Blue Excitation.

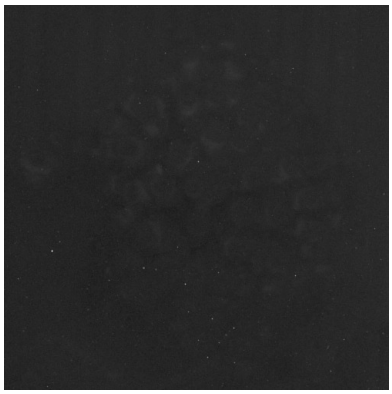

(c) Violet Excitation.

Fig. 8. Zoom of example images acquired during the dark and subsequent excitation phases of C1. The images exposition was enhanced to improve their visualization for the reader. The image acquired during the dark phase is in many ways similar to that which would be acquired with a classic imaging system not operating in fluorescence. In the dark image (6.a), only the calcareous structures, i.e., the corallites, are visible, while the living part of the coral, the polyps, are essentially indistinguishable from the background. On the other hand, in the Blue Excitation Fluorescence image (6.b), the polyps are clearly visible. Moreover, in figure 6.c, the violet excitation highlights the grown algae on the coral structure. All images were captured with water temperatures ranging from [18, 20] $^{\circ}$ and salinities ranging from [36, 38] %.)

IV. Discussion and Conclusions

Despite the significant benefits brought by photogrammetry and the notable progress of computer vision, to date, no measurement techniques have fully succeeded in the early detection of minor alterations of marine bioconstructors.

Fluorescence imaging has the potential to support and improve both ecological and physiological assessments. As discussed previously, our earlier studies validated the feasibility of monitoring the fluorescence emitted by GFP present in bioconstructors and established a correlation between health status and the fluorescence signal generated by GFP [28], [29]. In the current study, the system has been fully re-engineered to enable the analysis of fluorescence intensity produced by symbiotic algae within the corals, thereby allowing for the acquisition of much more comprehensive information. In addition to GFP-like proteins, chlorophyll represents a critical parameter, as it reflects the performance of the endosymbiotic algae sustaining the coral host. Indeed, coral health is often closely linked to the abundance of these symbionts within the tissues, with higher algal densities generally associated with more resilient colonies [39], [40]. Variations in chlorophyll fluorescence can thus act as sensitive early-warning signals of stress, anticipating bleaching events and their cascading consequences on coral physiology and resilience [30]–[32]. These characteristics highlight the value of chlorophyll as a marker for assessing coral health and vulnerability. When combined with GFP fluorescence, markers such as chlorophyll fluorescence can thus provide an integrated snapshot of the health status of corals and the stability of their symbiotic partnership [40].

As previously outlined, to fully leverage the potential offered by fluorescence imaging for monitoring marine bioconstructors, quantitative analysis is essential, and this requires metrological traceability. To facilitate straightforward and efficient traceability, we suggest correlating the fluorescence intensity measured by the system to a standard, the equivalent concentration of sodium fluorescein. This traceability will ensure consistency of results across different measuring systems and facilitate collaboration between multiple research groups. The aim of the proposed method is therefore to allow traceability while not intended to provide a direct estimate of the concentration of target fluorophores within bioconstructors.

The preliminary results demonstrate that the proposed measuring system can support both the corals identification and the detection of alterations in their state of health. As evident from Figure 8, the identification of polyps is easier in the fluorescence image. In the shown photo, it is possible to clearly distinguish the polyps. Figure 9 shows how the proposed device can quantifies fluorescence intensity. This enable comparative analysis between different coral samples and, more specifically, allows evaluation of the same coral sample at different time intervals, highlighting growth or decay. Figure 9a and Figure 9c highlight the polyps' GFP fluorescence, providing an idea of the amount of light they are emitting and a tool for counting polyps easily. Figure 9b and Figure 9d highlight the areas in which the endosymbiotic algae (zooxanthellae) were grown. Their presence is clearly visible in both corals, especially in C2, where the algae have grown up to the base on which the coral is mounted, producing that fluorescent rectangular region. Table II resumes the results of the tests. It is possible to observe a difference in the test of the two corallites. In fact, C1 showed a lower $MEFC_{SF-F}$ for both the fluorophores. This result is probably due to the difference in environmental conditions between the two measurements.

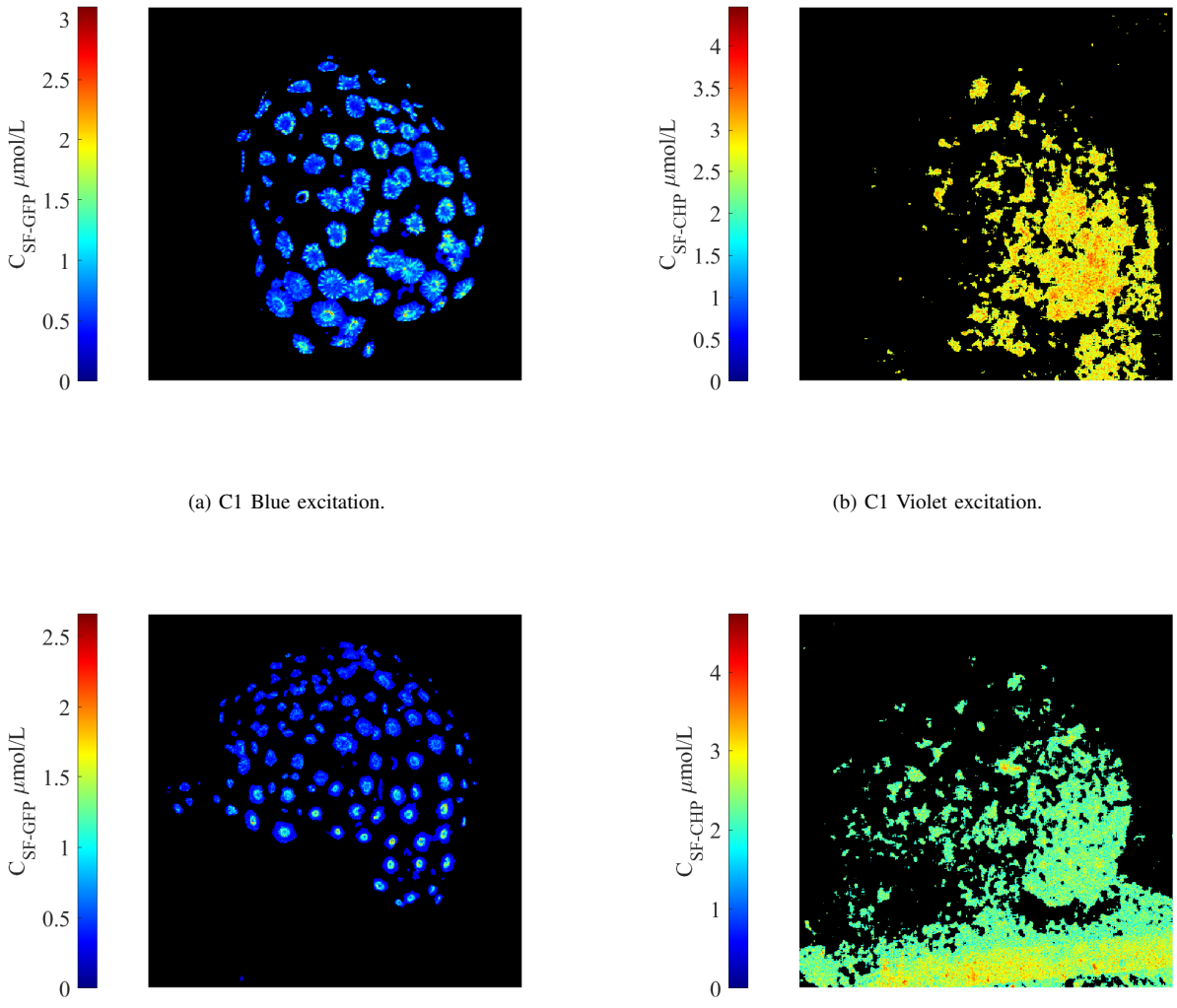

(a) C1 Blue excitation.

(b) C1 Violet excitation.

(c) C2 Blue excitation.

(d) C2 Violet excitation.

Fig. 9. Result of the fluorescence intensity analysis performed through the calibration curves of the instrument. The figure shows the excitation for both the corals and for both the fluorophores.

TABLE II
RESULTS OF THE EXPERIMENTAL TEST. MINIMUM DETECTABLE EQUIVALENT FLUORESCEIN CONCENTRATION $MEFC_{SF-F}$, CONCENTRATION THRESHOLD C_{th-F}, AVERAGE VALUES OF N_{pixel} AND $\bar{C}_{SF-F}(t)$ OBTAINED FOR EACH EXCITATION LIGHT AND FOR EACH CORAL.

	$MEFC_{SF-GFP}$	$MEFC_{SF-CHP}$	C_{th-GFP}	C_{th-CHP}	$N_{pixel-GFP}$	$N_{pixel-CHP}$	$\bar{C}_{SF-GFP}(t)$	$\bar{C}_{SF-CHP}(t)$
C1	18 nmol/L	190 nmol/L	$21 \cdot MEFC_{SF-GFP}$	$14 \cdot MEFC_{SF-CHP}$	15 %	16 %	620 nmol/L	2.76 µmol/L
C2	43 nmol/L	470 nmol/L	$6 \cdot MEFC_{SF-GFP}$	$\frac{9}{2} \cdot MEFC_{SF-CHP}$	10 %	35 %	400 nmol/L	2.36 µmol/L

Moreover, considering chlorophyll fluorescence, the number of pixels above the threshold C_{TH-CHP} is much higher for C2 instead of C1. This result is due to the presence of algae in the basement under the corallite.

Concluding, the reported results demonstrate that the proposed system offers measuring interval, stability, and repeatability likely suitable for analyzing marine bioconstructor colonies. However, given that, to the best of our knowledge, no fluorescence intensity values or thresholds have been defined to classify the health status of corals, it is currently not possible to establish the target uncertainty and, therefore, determine whether the performance offered by the proposed measuring system and method is actually capable of fully enabling early detection of alterations in marine colonies. Nonetheless, we believe that the simple method proposed in this study for metrological traceability can support the development of quantitative fluorescence imaging of bioconstructors and, therefore, contribute to the future complete determination of the required

metrological performance, thus favoring the widespread use of quantitative fluorescence imaging to monitor marine bioconstructors.

REFERENCES

[1] A. de la Torriente, R. Aguilar, J. M. González-Irusta, M. Blanco, and A. Serrano, "Habitat forming species explain taxonomic and functional diversities in a mediterranean seamount," *Ecological Indicators*, vol. 118, p. 106747, 2020.

[2] C. Cerrano, R. Danovaro, C. Gambi, A. Pusceddu, A. Riva, and S. Schiaparelli, "Gold coral (savalia savaglia) and gorgonian forests enhance benthic biodiversity and ecosystem functioning in the mesophotic zone," *Biodiversity and Conservation*, vol. 19, no. 1, pp. 153–167, 2010.

[3] T. Sobha, C. Vibija, and P. Fahima, "Coral reef: a hot spot of marine biodiversity," in *Conservation and sustainable utilization of bioresources*. Springer, 2023, pp. 171–194.

[4] G. Chimienti, D. De Padova, M. Adamo, M. Mossa, A. Bottalico, A. Lisco, N. Ungaro, and F. Mastrototaro, "Effects of global warming on mediterranean coral forests. sci rep 11: 20703," 2021.

[5] S. Righi, D. Prevedelli, R. Simonini *et al.*, "Ecology, distribution and expansion of a mediterranean native invader, the fireworm hermodice carunculata (annelida)," *Mediterranean Marine Science*, vol. 21, no. 3, pp. 558–574, 2020.

[6] G. E. Forrester, R. L. Flynn, L. M. Forrester, and L. L. Jarecki, "Episodic disturbance from boat anchoring is a major contributor to, but does not alter the trajectory of, long-term coral reef decline," *PloS one*, vol. 10, no. 12, p. e0144498, 2015.

[7] J. H. R. Burns, D. Delparte, R. D. Gates, and M. Takabayashi, "Utilizing underwater three-dimensional modeling to enhance ecological and biological studies of coral reefs," *The International Archives of the Photogrammetry, Remote Sensing and Spatial Information Sciences*, vol. 40, pp. 61–66, 2015.

[8] R. Ferrari, W. F. Figueira, M. S. Pratchett, T. Boube, A. Adam, T. Kobelkowsky-Vidrio, S. S. Doo, T. B. Atwood, and M. Byrne, "3d photogrammetry quantifies growth and external erosion of individual coral colonies and skeletons," *Scientific reports*, vol. 7, no. 1, p. 16737, 2017.

[9] P. Bongaerts, C. E. Dubé, K. E. Prata, J. C. Gijsbers, M. Achlatis, and A. Hernandez-Agreda, "Reefscape genomics: leveraging advances in 3d imaging to assess fine-scale patterns of genomic variation on coral reefs," *Frontiers in Marine Science*, vol. 8, p. 638979, 2021.

[10] C. Qiu, Z. Wu, S. Kong, and J. Yu, "An underwater micro cable-driven pan-tilt binocular vision system with spherical refraction calibration," *IEEE Transactions on Instrumentation and Measurement*, vol. 70, pp. 1–13, 2021.

[11] H. Du, D. Yao, S. Li, and Q. Zhang, "Ultrasonic measurement on the thickness of oil slick using the remotely operated vehicle (rov) as a platform," *IEEE Transactions on Instrumentation and Measurement*, vol. 72, pp. 1–10, 2023.

[12] J. Xia, T. Ma, Y. Li, S. Xu, and H. Qi, "A scale-aware monocular odometry for fishnet inspection with both repeated and weak features," *IEEE Transactions on Instrumentation and Measurement*, vol. 73, pp. 1–11, 2024.

[13] S. M. Nornes, M. Ludvigsen, and A. J. Sørensen, "Automatic relative motion control and photogrammetry mapping on steep underwater walls using rov," in *OCEANS 2016 MTS/IEEE Monterey*, 2016, pp. 1–6.

[14] R. Mendoza, D. Menacho, F. Cuellar, C. Carranza, and D. Arce, "Multicamera acquisition system for virtual model generation with underwater photogrammetry," in *OCEANS 2021: San Diego – Porto*, 2021, pp. 1–6.

[15] T. Treibitz, B. P. Neal, D. I. Kline, O. Beijbom, P. L. Roberts, B. G. Mitchell, and D. Kriegman, "Wide field-of-view fluorescence imaging of coral reefs," *Scientific reports*, vol. 5, no. 1, p. 7694, 2015.

[16] Y. Fu, W. Li, and M. Huang, "Ultrawide range of concentration measurement assisted by fluorescence intensity distribution imaging," *IEEE Transactions on Instrumentation and Measurement*, vol. 72, pp. 1–6, 2023.

[17] N. Wang, Y. Liu, and H. Li, "An efficient and fast, noninvasive, auto-fluorescence detection method for early-stage oral cancer," *IEEE Transactions on Instrumentation and Measurement*, vol. 71, pp. 1–11, 2022.

[18] Z. Gan, P. Wu, N. Zeng, F. Zou, B. Xiong, M. Du, Q. Bao, J. Li, and Y. Bai, "Highly sensitive cy3 fluorescence detection method for microarray based on ccd and led," *IEEE Transactions on Instrumentation and Measurement*, vol. 72, pp. 1–12, 2023.

[19] G. Bulgarea and M. Boukadoum, "A high-performance instrumentation system to measure the fluorescence kinetics of plants for in vivo photosynthesis research," *IEEE Transactions on Instrumentation and Measurement*, vol. 50, no. 3, pp. 679–689, 2001.

[20] W. Wan, D. Hua, J. Le, T. He, Z. Yan, and C. Zhou, "Study of laser-induced chlorophyll fluorescence lifetime measurement and its correction," *Measurement*, vol. 60, pp. 64–70, 2015.

[21] V. Raimondi, P. Di Maggio, A. Gonnelli, L. Palombi, R. V. de Vries, A. Ciapponi, and P. Corradi, "Remote sensing of plastic marine litter by means of fluorescence lidar," in *IGARSS 2023 - 2023 IEEE International Geoscience and Remote Sensing Symposium*, 2023, pp. 1733–1735.

[22] Z. Li, P. Sun, H. Huang, W. Cai, X. Jiang, P. Guo, J. Fan, S. Zhang, J. Chen, J. Song, and H. Huang, "A compact and sensitive metal-capillary fluorometer: Application to online monitoring oil spill," *IEEE Transactions on Instrumentation and Measurement*, vol. 74, pp. 1–7, 2025.

[23] Q. Sun, W. Liu, C. Wen, and L. Cai, "Estimation of marine oil spill surface characteristics based on laser-induced fluorescence with ia-dbscan," *IEEE Transactions on Instrumentation and Measurement*, vol. 73, pp. 1–14, 2024.

[24] G. Ding, J. Wang, P. Tian, J. Zhang, J. Zou, Y. Wu, X. Wu, and X. Pan, "A novel handheld high-throughput device for rapid detection of phytoplankton in ship's ballast water," *IEEE Transactions on Instrumentation and Measurement*, vol. 70, pp. 1–13, 2021.

[25] K. Pan, X. Luan, B. Li, H. Yu, J. Wu, S. Li, and Q. Li, "Quasi-3d fluorescence spectroscopy for rapid on-site algae species analysis (july 2025)," *IEEE Sensors Journal*, pp. 1–1, 2025.

[26] J. Kissinger and D. Wilson, "Portable fluorescence lifetime detection for chlorophyll analysis in marine environments," *IEEE Sensors Journal*, vol. 11, no. 2, pp. 288–295, 2011.

[27] M. S. Roth and D. D. Deheyn, "Effects of cold stress and heat stress on coral fluorescence in reef-building corals," *Scientific Reports*, vol. 3, no. 1421, pp. 1–8, 2013.

[28] P. Rossi, S. Righi, L. Parente, C. Castagnetti, S. Cattini, G. Di Loro, E. Falvo, F. Grassi, F. Mancini, L. Rovati *et al.*, "Photogrammetric and fluorescence solutions for monitoring of habitat forming organisms," *International Archives of the Photogrammetry, Remote Sensing and Spatial Information Sciences*, vol. 43, no. 2-2022, pp. 877–883, 2022.

[29] C. Castagnetti, P. Rossi, S. Righi, S. Cattini, R. Simonini, L. Rovati, and A. Capra, "Potentialities of the combined use of underwater fluorescence imagery and photogrammetry for the detection of fine-scale changes in marine bioconstructors," *Frontiers in Marine Science*, vol. 10, p. 1305807, 2024.

[30] R. V. Thurber, D. Willner-Hall, B. Rodriguez-Mueller, C. Desnues, R. A. Edwards, F. Angly, E. Dinsdale, L. Kelly, and F. Rohwer, "Metagenomic analysis of stressed coral holobionts," *Environmental microbiology*, vol. 11, no. 8, pp. 2148–2163, 2009.

[31] A. G. Grottoli, M. E. Warner, S. J. Levas, M. D. Aschaffenburg, V. Schoepf, M. McGinley, J. Baumann, and Y. Matsui, "The cumulative impact of annual coral bleaching can turn some coral species winners into losers," *Global change biology*, vol. 20, no. 12, pp. 3823–3833, 2014.

[32] C. Carbonne, S. Comeau, K. Plichon, S. Schaub, J.-P. Gattuso, and N. Teixidó, "Response of two temperate scleractinian corals to projected ocean warming and marine heatwaves," *Royal Society Open Science*, vol. 11, no. 3, p. 231683, 2024.

[33] Z. Wang, W. Wang, Y. Zhang, L. Zhang, D. Liu, Y. Gao, and Y. Liu, "Variable chlorophyll a fluorescence techniques to determine photosynthetic activity of marine phytoplankton," in *2017 Chinese Automation Congress (CAC)*, 2017, pp. 7096–7098.

[34] T. Hou, H. Chang, H. Jiang, P. Wang, N. Li, Y. Song, and D. Li, "Smartphone based microfluidic lab-on-chip device for real-time detection, counting and sizing of living algae," *Measurement*, vol. 187, p. 110304, 2022.

[35] J. R. Lakowicz, *Topics in fluorescence spectroscopy: principles*. Springer Science & Business Media, 1992, vol. 2.

[36] ——, *Principles of fluorescence spectroscopy*. Springer, 2006.

[37] Z. Liu, Y. Bi, W. Chu, W. Li, and P. Wang, "Inner filter effect correction for fluorescence detection in auc by difference invariant," *IEEE Transactions on Instrumentation and Measurement*, vol. 74, pp. 1–7, 2025.

[38] S. Cattini and L. Rovati, "A simple measuring system and calibration method to investigate light transmission ability of light-transmitting fiber posts," in *2015 IEEE International Instrumentation and Measurement Technology Conference (I2MTC) Proceedings*. IEEE, 2015, pp. 1141–1146.

[39] A. Apprill, R. Bidigare, and R. Gates, "Visibly healthy corals exhibit variable pigment concentrations and symbiont phenotypes," *Coral Reefs*, vol. 26, no. 2, pp. 387–397, 2007.

[40] J. Teague, J. Willans, D. A. Megson-Smith, J. C. Day, M. J. Allen, and T. B. Scott, "Using colour as a marker for coral 'health': A study on hyperspectral reflectance and fluorescence imaging of thermally induced coral bleaching," in *Oceans*, vol. 3, no. 4. MDPI, 2022, pp. 547–556.